ELSEVIER

Journal of Molecular Graphics and Modelling 21 (2002) 19–27

Journal of Molecular Graphics and Modelling

www.elsevier.com/locate/JMGM

Motion of an antiviral compound in a rhinovirus capsid under rotational symmetry boundary conditions

Shigetaka Yoneda [a,*], Teruyo Yoneda [b,1], Youji Kurihara [b], Hideaki Umeyama [b]

[a] *School of Science, Kitasato University, 1-15-1 Kitasato, Sagamihara-shi, Kanagawa-ken 228-8555, Japan*
[b] *School of Pharmaceutical Sciences, Kitasato University, Tokyo, Japan*

Accepted 7 December 2001

Abstract

A molecular dynamics (MD) simulation of a complex of a rhinovirus protein shell referred to as a "capsid" and an anti-rhinovirus drug, WIN52084s, was performed under the rotational symmetry boundary conditions. For the simulation, the energy parameters of WIN52084s in all-atom approximations were determined by ab initio calculations using a 6-31G* basis set and the two-conformational two-stage restricted electrostatic potential fit method. The motion of WIN52084s and the capsid was focused on in the analysis of the trajectory of the simulation. The root mean square deviations of WIN52084s from the X-ray structure were decomposed to conformational, translational, and rotational components. The translation was further decomposed to radial, longitudinal, and lateral components. The conformation of WIN52084s was rigid, but moving in the pocket. The easiest path of motion for WIN52084s was on the longitudinal line, providing a track for the binding process required of the anti-rhinovirus drug to enter the pocket. The conformation of the pocket was also preserved in the simulation, although the position of the pocket in the capsid fluctuated in the lateral and radial directions.

Keywords: Molecular dynamics simulation; WIN52084s; Picornavirus; Uncoating; Common cold

1. Introduction

Virus protein shells named "capsids" are not only containers of viral genomes, but are also elaborate mechanisms that emerge from host cells, travel under severe environmental conditions, attach to other host cells, and release the viral genomes for further viral multiplication [1]. These elaborate capsid mechanisms have been extensively studied in detail especially for small viruses, because X-ray coordinates of capsids can be determined for structure-based studies. The capsids of a rhinovirus and other picornaviruses are one example of such well-studied viral mechanisms.

A rhinovirus capsid is a spherical protein shell with diameter of 300 Å. The capsid has icosahedral symmetry and is composed of 60 identical copies of a protein unit called "protomer," which is composed of four peptide chains designated as "VP1," "VP2," "VP3," and "VP4." Attachment of a rhinovirus capsid to a host cell receptor is believed to trigger a global structural change in the capsid, resulting in a large hole at the five-fold axis, and the rhinoviral RNA genome contained inside is released through the hole [2]. This global structural change designated as starting "uncoating" is related to a small hydrophobic molecule referred to as a "pocket factor." The binding site of the pocket factor is a long, narrow, and hydrophobic cavity called a "pocket," which is located beneath a "canyon," a depression designated on the capsid surface. A rhinovirus capsid is usually bound with the pocket factor before attaching to receptors. The pocket factor stabilizes the capsid structure. The attachment of the capsid to receptors is believed to cause the release of the pocket factor, thereby initiating a global structural change in the capsid, resulting in uncoating.

Numerous compounds that mimic the pocket factor have been synthesized for biological and pharmaceutical purposes [2,3]. Many of the compounds strongly bind themselves in the pockets of rhinovirus capsids and other picornavirus capsids so that they are not released from the capsids even after the attachment of capsids to host cells. The binding of these compounds is believed to entropically stabilize the capsid structures and prevent the structural changes in uncoating [4–9]. The compounds sometimes prevent attachment to host cells. WIN52084s, shown in Fig. 1, is one of the capsid-binding drugs, and it has often been regarded as

* Corresponding author. Tel.: +81-42-778-9404; fax: +81-42-778-9953.
E-mail address: shigetaka.yoneda@nifty.ne.jp (S. Yoneda).
[1] Present address: PharmaDesign, Inc., 4-2-10 Hatchobori, Chuo-ku, Tokyo 104-0032, Japan.

1093-3263/02/$ – see front matter
PII: S1093-3263(02)00105-5

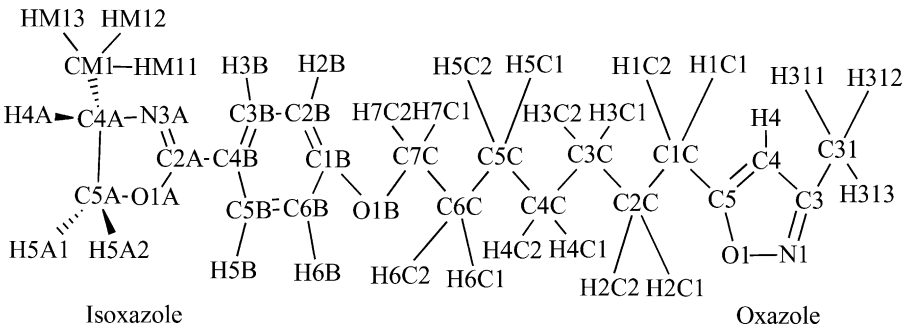

Fig. 1. Chemical structure of WIN52084s.

a typical one of these drugs, since the X-ray coordinates of a complex of rhinovirus capsid and WIN52084s were determined early on. WIN52084s is a flexible molecule with an alkyl chain between aromatic rings and is forced to intrude into the narrow pocket. Because the binding free energy is of the first importance in the binding processes, many studies have focused on thermodynamics [7]. Thus, if motional properties of WIN52084s and the capsid are analyzed in detail additionally, the binding can be more deeply clarified. We address in this article, a molecular dynamics (MD) simulation of a complex of rhinovirus capsids and WIN52084s using the rotational symmetry boundary condition to investigate the motion of WIN52084s and the pocket.

The rotational symmetry boundary conditions are described in detail in previous articles [7,8,10–13], and we explain it only briefly here. The rotational symmetry boundary conditions are used as a method for accelerating the calculations for large symmetric molecular assemblies such as a virus capsid. Because of the heavy computational load, most simulation-based studies on capsids have been restricted to small regions near the pocket, and motion in other parts of the capsid has been neglected. In contrast, a simulation under the rotational symmetry boundary conditions is equivalent to a simulation of an entire capsid with the constraint of perfectly icosahedral symmetry, and inter-protomer interactions and the motion of the entire capsid can be correctly calculated using the icosahedral symmetry. Furthermore, a simulation under rotational symmetry boundary conditions has to process only a single protomer, and thus, the simulation is highly accelerated. In previous methodological articles, we formulated the rotational symmetry boundary condition by using the proposed basic equations, referred to as "protomer number equations," and performed MD simulations on a rhinovirus capsid and on a crystal of glycogen phosphorylase in $P4_32_12$ symmetry [11,12].

Because protein is flexible [14–16], the position of WIN52084s and the pocket can be moving enough in the whole capsid structure to have some roles in viral processes. Since calculational analyses on the conformation of WIN52084s and the pocket was already reported as well as energetic analyses [17–21], we focus on the molecular translation of WIN52084s and the pocket in the capsid. The method of using rotational symmetry boundary condition works by not neglecting the effect of any neighboring residues, so it is an appropriate method for this analysis.

2. Methods

We developed the energy parameters of WIN52084s in all-atom approximations, because all of the previous energy parameters of WIN52084s [6,18,20,21] were in united-atom approximations, when we started the study. A set of all-atom energy parameters was reported in a recent study [8], in which rather small charges were used for some atoms including C2A. The Lennard–Jones parameters and the parameters of bond, angle, and torsion were derived from the C96 parameters of AMBER [22,23] and the previous parameters in united-atom approximations. We used the 2rs1 structure [24], for a complex of a rhinovirus capsid and WIN52084s deposited to the protein databank [25]. The WIN52084s structure was fully optimized with Gaussian'98 [26] using a STO-3G basis set. Electrostatic potentials were calculated using a 6-31G* basis set at 2176 grids around the X-ray structure and at 2101 grids around the fully optimized structure. The sum of the squares of the electrostatic potentials at all 4277 grids was 0.903, where 27.21 V was defined as the unit used to express the electrostatic potential. The two-conformational two-stage fit technique of the restrained electrostatic potential fit method [27,28] was applied to these electrostatic potentials, using the RESP module of the AMBER program package [29]. The sum of the square errors, $\sum(V_i - V_i^c)^2$, was 0.031 in the final stage of the fit, where V_i is the electrostatic potential calculated by the ab initio calculation and V_i^c is that calculated by the Coulomb equation from the fitted atomic charges. Table 1 lists the atomic charges that were subsequently determined. We also determined the energy parameters for the torsion angle of –C4B–C2A–, because C4B–C2A is a bond connecting two aromatic rings that is not included in any amino acids or nucleic acids. The torsion angle of –C4B–C2A– in the fully optimized structure was rotated by 15° intervals, and the energy of each of the generated structures was

Table 1
Atom types and charges of WIN52084s

Name	Type	Charge
O1	OS	−0.128
N2	NB	−0.461
C3	CC	0.539
C31	CT	−0.322
H311	HC	0.103
H312	HC	0.103
H313	HC	0.103
C4	C*	−0.521
H4	HA	0.189
C5	CC	0.306
C1C	CT	−0.010
H1C1	HC	0.032
H1C2	HC	0.032
C2C	CT	0.010
H2C1	HC	0.014
H2C2	HC	0.014
C3C	CT	−0.043
H3C1	HC	0.017
H3C2	HC	0.017
C4C	CT	−0.038
H4C1	HC	0.022
H4C2	HC	0.022
C5C	CT	−0.034
H5C1	HC	0.035
H5C2	HC	0.035
C6C	CT	−0.021
H6C1	HC	0.029
H6C2	HC	0.029
C7C	CT	0.042
H7C1	H1	0.056
H7C2	H1	0.056
O1B	OS	−0.348
C1B	CA	0.255
C2B	CA	−0.198
H2B	HA	0.138
C3B	CA	−0.087
H3B	HA	0.151
C4B	CA	−0.149
C5B	CA	−0.172
H5B	HA	0.151
C6B	CA	−0.124
H6B	HA	0.138
C2A	CC	0.740
N3A	NB	−0.794
C4A	CT	0.412
H4A	H1	0.009
CM1	CT	−0.306
HM11	HC	0.077
HM12	HC	0.077
HM13	HC	0.077
C5A	CT	0.047
H5A1	H1	0.048
H5A2	H1	0.034
O1A	OS	−0.403

calculated using a 6-31G* basis set. The empirical function of the torsion potential of –C4B–C2A– was determined as $4.0(1.0 + \cos(2\phi + 180))$ by a minor calculation of fitting to the ab initio energy. The effect of one to four interactions in the fitting was negligible.

An MD simulation on the rhinovirus capsid with WIN52084s was performed using the APRICOT program [30]. The initial structure was the X-ray structure, 2rs1. All of the ordered water atoms were included. Because three of the four chains lack the N-terminals by disorder, the acetyl (ACE) residues of the AMBER parameter were added to the trimmed N-terminals. The C96 energy parameters of AMBER and the TIP3P potentials were used for protein and water, respectively. The numbers of atoms in protein, water, and WIN52084s were 12458, 24, and 54, respectively. The X-ray structure was optimized with positional constraints of 300 kcal/(mol Å^2) on all of the atoms except hydrogen and ACE. A dielectric constant of 1 and a cutoff of 15 Å were adopted. The distance of the protein atoms from the center of the capsid symmetry was between 106 and 162 Å. Thus, the region at a distance of 86–183 Å from the center was considered as a water zone, and the zone was filled with additional water molecules. The number of the added water atoms was 22296. A simple half-harmonic potential with 1.0 kcal/(mol Å^2) was added to draw water molecules back into the water zone. The structure of this system was optimized for all atoms except hydrogen, ACE, and the added water under the rotational symmetry boundary conditions with the positional constraints of 300 kcal/(mol Å^2). Furthermore, an 80 ps MD simulation using the same positional constraints in the rotational symmetry boundary conditions was performed to equilibrate the structure and dynamics of water. Neighbor lists were generated at 20-step intervals. SHAKE [31] for bonds to hydrogen atoms and a time step of 2 ps were applied. The initial temperature was 100 K and temperature was kept constant at 300 K with a relaxation time of 0.5 ps [32]. The conditions related to the rotational symmetry boundary conditions were equal to those adopted in a previous study [11]. Using the final coordinates and velocities of the equilibration run, a 200 ps MD simulation without positional constraints was performed. The procedure to stop the parallel translation and rotate of the whole protein structure was not followed, because the protomer is a sub-structure in the whole capsid.

The root mean square (rms) deviations of a molecule from the X-ray structure in the MD simulation were decomposed into conformational, translation, and rotational components. The conformational component is the rms deviations after least square fitting. The translational component is defined as the length of movement of the center of the molecule. The remainder is the rotational component and the sum of the squares of the three components is equal to the rms deviations before the least square fitting.

To analyze the direction of translation, we defined three unit vectors: $\boldsymbol{R}$, $\boldsymbol{T}$, and $\boldsymbol{P}$. $\boldsymbol{R}$ is directed from the center of capsid symmetry to the center of the X-ray structure of WIN52084s. $\boldsymbol{T}$ is directed from C1B of the phenoxy ring to C3 of the oxazole ring in the X-ray structure of WIN52084s, and it is set orthogonal to $\boldsymbol{R}$ by Schmidt's orthogonalization method. $\boldsymbol{T}$ is directed approximately from the entrance pore to the interior end of the binding pocket. $\boldsymbol{P}$ is defined as the

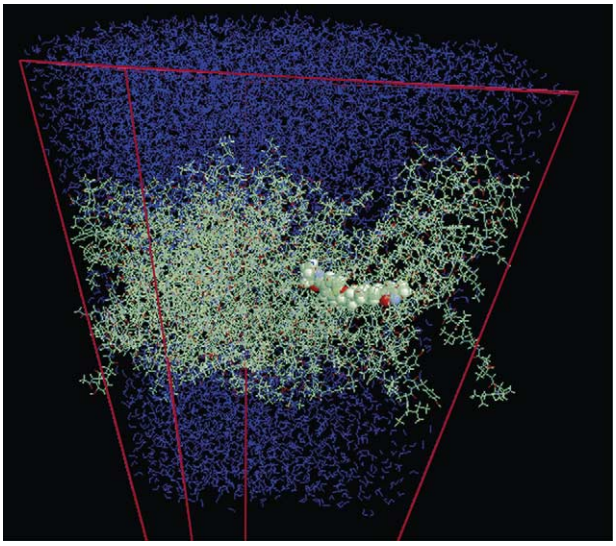

Fig. 2. Final snapshot of MD simulation of rhinovirus capsid protomer bound with WIN52084s. Water molecules are indicated in blue. The red lines denote the edges of an asymmetric unit of icosahedral symmetry, and the unit is referred to as a "computational cell" in the rotational symmetry boundary method [11]. The vertices of the computational cell are at a distance of 180 Å from the center of symmetry. WIN52084s is drawn as a space-fill model.

outer product of $\boldsymbol{R}$ and $\boldsymbol{T}$ (i.e. $\boldsymbol{R} \times \boldsymbol{T}$). Thus, $\boldsymbol{R}$ represents the radial, $\boldsymbol{T}$ represents the longitudinal, and $\boldsymbol{P}$ represents the lateral directions of WIN52084s. Using these three vectors, we decomposed a translation into radial, longitudinal, and lateral components. The sum of the squares of the radial, longitudinal, and lateral components is equal to the square of the translational component of rms deviations.

3. Results

Fig. 2 is the final snapshot of the MD simulation. WIN52084s binds in the capsid protomer, and the protomer is covered with a thick layer of water. The rms deviations of the protomer from the X-ray structure were calculated using the MD trajectory, considering all atoms except hydrogens and ACE residues, whose coordinates are not written in the X-ray file. Thus, our rms calculation gives larger values for the same structural difference than when only the backbone atoms or only the atoms with small experimental B-factors are considered. As described in the Section 2, the rms deviations from the X-ray structure are decomposed to the conformational, translational, and rotational components. Table 2 lists the components that are shown for the protomer in Fig. 3a. The total rms deviations of the protomer during the final 50 ps was 2.04 Å and the conformational component was 1.91 Å, indicating good precision in the simulation of this large protein. In addition, some translational components had a value as great as 0.67 Å, and the rotational component was only 0.22 Å. As shown in Table 2, the time

Table 2
Time average of rms deviations from the X-ray structure during final 50 ps

	Total	Conformational	Translational	Rotational
Protomer	2.04	1.91	0.67	0.22
Pocket	1.49	1.15	0.89	0.27
WIN52084s	1.43	0.69	1.03	0.68

average of the conformational deviation of the pocket during the final 50 ps is 1.15 Å, which is much smaller than the average of 1.91 Å for the protomer. The final structure and X-ray structure of the pocket are shown in Fig. 4. The pocket residues were selected using a distance criterion, as

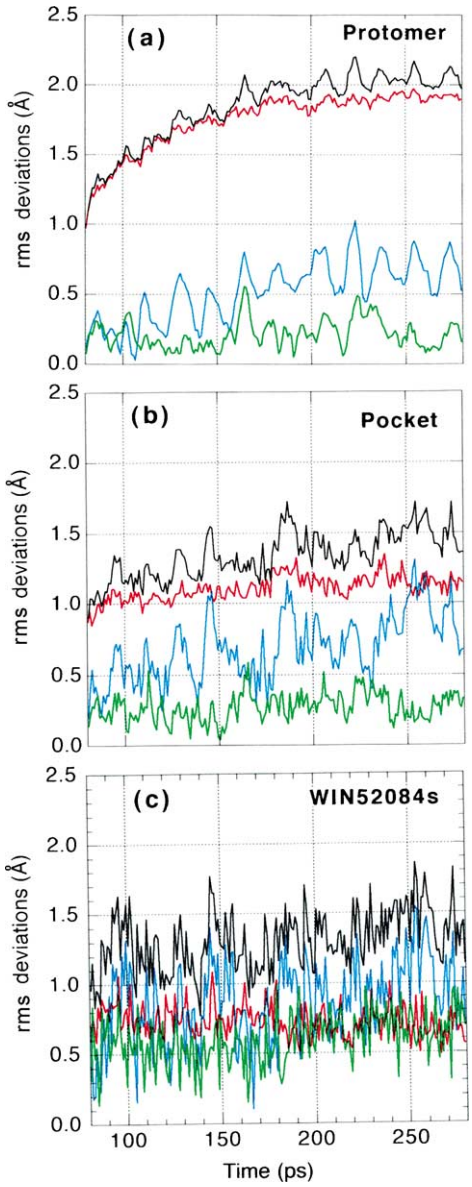

Fig. 3. Time profile of the rms deviations of: (a) the capsid protomer, (b) the pocket, and (c) WIN52084s. The total deviation (black) is decomposed to the conformational (red), translational (cyan), and rotational (green) components. Pocket residues are defined in Fig. 4.

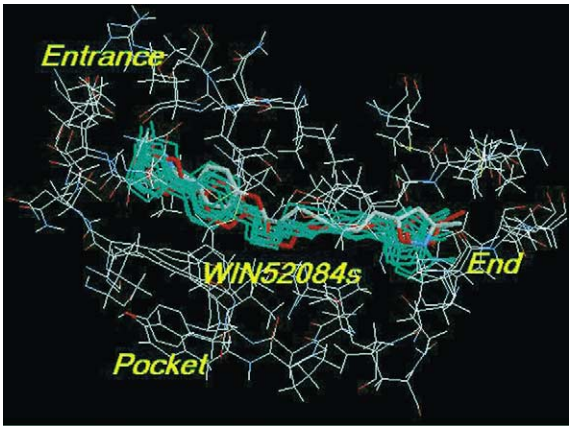

Fig. 4. Superimposed snapshots of WIN52084s and pocket. The final snapshot at 280 ps is shown in red, and the X-ray structure of WIN52084s is shown in the CPK colors. Another nine snapshots at 20 ps intervals are shown in cyan. The X-ray structure and the final structure of the pocket residues are in thin wire-frames. The pocket residues were selected based on a criterion that the contact distance to WIN52084s in the X-ray structure must be shorter than 6.0 Å. The numbers of the residues and atoms of the pocket are 33 and 261, respectively. The hydrogen atoms of WIN52084s are not shown. The direction of view is identical to that in Fig. 2.

explained in the caption of Fig. 4. The small conformational deviation of the pocket caused the total deviation of the pocket to be smaller than that of the protomer, as indicated in Table 2 and Fig. 3b. The average translational deviation of the pocket is 0.89 Å, which is larger than the average of 0.67 Å for the protomer. The average rotational deviation is similar to that of the protomer. The conformational deviation of WIN52084s is very small at 0.69 Å, decreasing the total deviation of WIN52084s, which was already smaller than the total deviations of the protomer and pocket, as shown in Fig. 3c and Table 2. WIN52084s has the translational deviation of 1.03 Å and rotational deviation of 0.68 Å during the final 50 ps, and these deviations are larger than those of the protomer and pocket.

The decomposition of translation described in the Section 2 was carried out on WIN52084s. To clarify the translation relative to the pocket position, the value of the WIN52084s translation was subtracted by the value of the pocket translation prior to the decomposition. Thus, in the translation values shown in Fig. 5c, motion of the pocket is filtered out. The sum of the radial, longitudinal, and lateral components of WIN52084s translation is calculated so that it is not equal to the translational rms deviation of WIN52084s relative to the pocket. Table 3 shows that the averages of the radial, longitudinal, and lateral translations of WIN52084s relative to the pocket during the final 100 ps were −0.02, −0.39, and 0.18 Å, respectively, and their fluctuations are 0.20, 0.25, and 0.16 Å, respectively. Therefore, during the MD simulation, WIN52084s translated primarily in the longitudinal direction by 0.39 Å for the entrance pore of the pocket from the inner end and the translational fluctuation was the largest fluctuation in the longitudinal direction. Fig. 6c shows the

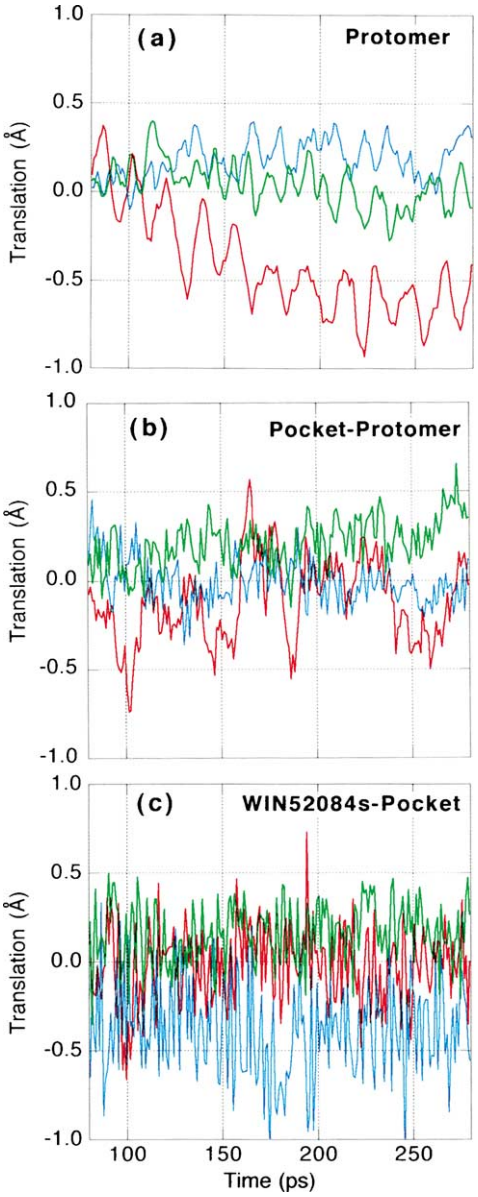

Fig. 5. Translations of: (a) the capsid protomer, (b) the pocket relative to the protomer, and (c) WIN52084s relative to the pocket. Each translation is decomposed to radial (red), longitudinal (cyan), and lateral (green) components.

Table 3
Time average of translation during final 100 ps[a]

	Radial	Longitudinal	Lateral
Protomer	−0.61 (0.14)	0.21 (0.10)	−0.02 (0.11)
Pocket[b]	−0.10 (0.20)	−0.04 (0.10)	0.26 (0.13)
WIN52084s[c]	−0.02 (0.20)	−0.39 (0.25)	0.18 (0.16)

[a] Values in parentheses are the standard deviations.
[b] Translation relative to the capsid.
[c] Translation relative to the pocket.

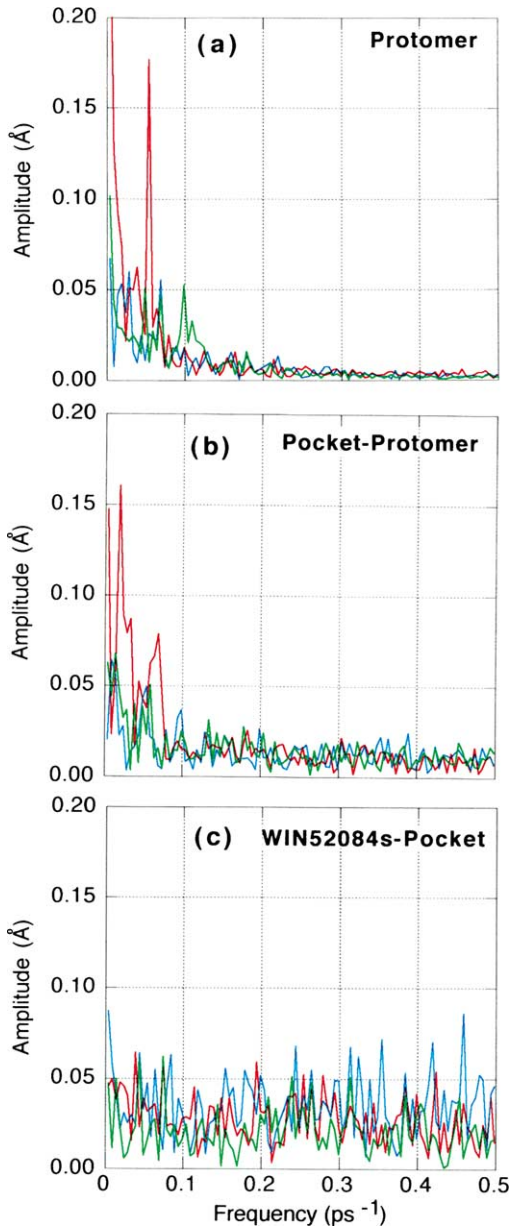

Fig. 6. Fourier amplitude of translational motion. The amplitudes of the radial, longitudinal, and lateral translations are denoted in red, cyan, and green, respectively. The amplitudes for: (a) the protomer, (b) the pocket, and (c) WIN52084s were calculated by the Fourier expansion of the values in Fig. 5.

Fourier amplitudes of the values in Fig. 5c. The Fourier spectrum is approximately flat, similar to white noise, without a prominent peak.

The pocket translation was also decomposed to the three components of WIN52084s that are in the radial, longitudinal, and lateral directions. To clarify the translation relative to the protomer position, the value of the pocket translation was subtracted by the value of protomer translation, prior to the decomposition. Fig. 5b shows the three components during the MD simulation. Table 3 shows that the averages of the radial, longitudinal, and lateral components in the translation of the pocket in the capsid during the final 100 ps were −0.10, −0.04, and 0.26 Å, respectively. Their rms fluctuations were 0.20, 0.10, and 0.13 Å, respectively. The position of the pocket translated primarily in the lateral direction by 0.26 Å during the MD simulation, although the pocket was fluctuating primarily in the radial direction. Fig. 6b shows the Fourier amplitudes of translations calculated with the values in Fig. 5b. The Fourier amplitudes of translation in Fig. 6b are damping at higher frequencies and there are some high peaks at lower frequencies.

The protomer translation was also decomposed to the three components of WIN52084s that are in the radial, longitudinal, and lateral directions, as shown in Fig. 5a. Table 3 lists the averages of −0.61 Å for the radial component, 0.21 Å for the longitudinal one, and −0.02 Å for the lateral one during the final 100 ps. Their rms fluctuations were 0.14, 0.10, and 0.11 Å, respectively. Therefore, the averaged translation of the capsid protomer in the MD simulation is mainly directed toward the center of icosahedral symmetry, and fluctuations in the translations are similar in the three directions. Fig. 6a shows a Fourier analysis of the translations of Fig. 5a. The Fourier amplitudes of translation are damping at higher frequencies. The highest peak is at a frequency of 0.005 ps^{-1} (period of 200 ps) for all three components. There is another prominent peak of the radial component, indicated in red at frequency of 0.055 ps^{-1} (period of 18 ps).

4. Discussion

As indicated in Table 2 and Fig. 3c, the conformation of WIN52084s was rigid and well equilibrated in this large MD simulation. The translational motion of WIN52084s in the pocket was small, and there were no prominent Fourier peaks that dominated the fluctuation, as shown in Fig. 6c. Consequently, the translational motion was quickly equilibrated in the MD simulation.

In an early simulation of rhinovirus capsid [19], moving kink waves were observed on the alkyl chain of WIN52084s, and the alkyl chain had a large thermal motion at the oxazole end. Furthermore, in a study [21] of 200 ps simulations of a rhinovirus capsid bound with WIN53338, which is analogous to WIN52084s, the aliphatic chain was flexible and the isoxazole and oxazole rings were able to rotate. In contrast, the WIN compounds bound with the capsid was more rigid in our simulation, as described earlier. We used the rotational symmetry boundary conditions, the non-bonded cutoff of 15 Å, which is much longer than the cutoffs of about 8 Å adopted in the previous studies, and the all-atom energy parameters of WIN52084s. Naturally, the X-ray structure is expected to be better conserved because of the high precision of calculations in simulations nowadays. However, the flexible feature of the alkyl chain of the WIN compounds in previous studies was reproduced in our MD simulation, and the torsion angles of the alkyl chain of WIN52084s were flexible, as shown in Fig. 4.

Atomic deviations are generally larger in shallow local minima in the less rugged energy landscape of united-atom parameters. Therefore, the all-atom parameters that we developed for of WIN52084s are better for longer and more realistic simulations, and the united-atom parameters can be more useful as a simplified model for investigating long-time-scale phenomena requiring only limited computer processing time.

The averaged position of WIN52084s changed by −0.39 Å in the longitudinal direction (i.e. for the entrance pore of the pocket beginning from the inner end). In a previous study, on a rhinovirus capsid bound with WIN53338 [21], there was also a tendency for the WIN drug to shift along the binding pocket in the direction of the entrance pore. The length of the shift and the amplitudes of other deviations were much larger than those in our simulation. To investigate the movement of the WIN drugs in more detail, we performed another short MD simulation, because trajectories in MD simulations can be dependent on calculational parameters and initial conditions. Adopting the use of the united-atom energy parameters of WIN52084s reported in previous articles [6,18], an 80 ps equilibration run and a 50-ps sampling run were performed under the same calculational conditions described in the Section 2. The average translation of WIN52084s in the pocket was −0.18 Å in the radial direction, 0.45 Å in the longitudinal one, and −0.17 Å in the lateral one, in the short simulation. Their rms fluctuations were 0.21, 0.43, and 0.24 Å, respectively. The translation and fluctuation of WIN52084s were primarily on the longitudinal line, but the direction of translation was inverted for the end of pocket from the entrance. According to all of the results, the WIN compounds can easily move and fluctuate in both the positive and negative directions on the longitudinal line. This characteristic is consistent with the view that the WIN compounds are fluctuating around the X-ray structure in the narrow and long pocket of a capsid. The motion is restricted in the radial and lateral directions by the pocket wall, but the motion on the longitudinal line is easier in the direction of the geometrically and energetically flexible end and entrance. Although direct study on the entire binding process of the WIN compounds may not be possible in an MD simulation, the observed motion on the longitudinal line may indicate a track used for the binding process.

The spectrum of translation of pocket shown in Fig. 6b is not completely white noise, but the Fourier amplitudes are larger at lower frequencies, reflecting the slow translation of the pocket position in the capsid during the simulation. Because translation of residues in a capsid is equivalent to the conformational change of the capsid structure, the non-equilibrated slow translation of the pocket reflects the change of the capsid conformation, which was not well equilibrated in the simulation, as shown in Fig. 3a. In contrast, Fig. 3b shows that the structure of the pocket was better conserved in the simulation. Therefore, the structure of the pocket was more rigid and was moving in the capsid structure. Whereas WIN52084s fluctuated on the longitudinal line, the motion of the pocket was mainly perpendicular to the longitudinal direction, as shown in Table 3.

For a simple analysis from energetic view point, we calculated the non-bonded potential energy of WIN52084s during the simulation. We divided the last 80–280 ps of the simulation into the first period of 80–147 ps, the second period of 147–213 ps, and the final period of 213–280 ps. The averaged Lennard–Jones potentials for the first, second, and final periods were 68.6 (246.3), 235.4 (505.4), and 297.8 (407.1) kcal/mol, respectively, where the rms deviations of the potential are written in the parentheses. This increase of the Lennard–Jones potential was caused by the increase of the probability of occasional appearance of short contacts between WIN52084s and the pocket, indicating the adjustment of the position of pocket atoms to narrow the cavity size during the simulation. This narrowing corresponds to the very slow change of the conformational rms deviations of the pocket. There were no significant increase of the Lennard–Jones potential like this in other parts of capsid. The large fluctuation of the Lennard–Jones potential in the later periods indicates the entropic property of the interaction between WIN52084s and the capsid in equilibrated states, although more detailed energetic analysis should be necessary for clear discussion. The averaged electrostatic potentials of WIN52084s also increased, since they were −3.7 (14.2), 7.1 (12.0), and 10.5 (8.4) kcal/mol, for the first, second, and final periods, respectively. There was no clear correlation between the motion and the energy of WIN52084s.

The conformation and position of the protomer continued changing, as shown in Figs. 3a and 5a and as indicated in Tables 2 and 3. They were not well equilibrated in this MD simulation with a total time of 280 ps. The continuously changing position of the protomer is shown in Fig. 6a as the highest Fourier peaks at 0.005 ps^{-1}. Therefore, the conformation and translation of the protomer should be studied in longer and better-equilibrated simulations. However, Fig. 5a shows a clear feature of the protomer to translate by −0.61 Å in the radial direction (i.e. by 0.61 Å toward the center of icosahedral symmetry). This translation is equivalent to a size reduction of the entire capsid, because all protomers in the capsid are expected to move symmetrically under rotational symmetry boundary conditions. Because the X-ray coordinates of the RNA genome that is packed inside a rhinovirus capsid have not been determined by disorder, the RNA structure was not included in the MD simulation. Therefore, the tendency of the capsid to shrink may be a result of omitting the inner RNA structure. A rhinovirus produces naturally empty capsids lacking the RNA genome inside [1]. The effect of the inner RNA on the capsid size can be experimentally detected by very precisely comparing the sizes of a mature capsid and a natural empty capsid. Another clear feature of protomer dynamics is shown in Fig. 6a: the prominent peak of the radial translation with an amplitude of 0.18 Å at a frequency of 0.055 ps^{-1}. This indicates oscillation of the size of the

entire capsid with a period of 18 ps. According to the fundamental elastic theory and the elastic constants of common solids, the oscillation can be explained as a standing wave in a simple elastic shell, as shown in the Appendix A. Thus, such fast and small oscillations should be possible for any virus capsids, although more detailed analyses including an investigation on the effects of the water boundary are necessary to explain the cause within the calculation of the 18 ps oscillation. The oscillation of an entire capsid may be related to the global conformational change of the capsid, resulting in uncoating, and attachment to host cells.

The rotational symmetry boundary conditions were adopted for use in this work. Thus, the analyses on the conformation and translation of WIN52084s and the pocket were not badly affected by the neglect of the surrounding neighboring residues during this study. If the neighboring residues were omitted or their positions were fixed, correct analysis would have been impossible, especially for the translational properties. Furthermore, the analysis on the translation of the protomer, including the size reduction and oscillation of the entire capsid was possible in this work only by performing the simulation under the rotational symmetry boundary conditions, because it is impossible to investigate the translational motion of a capsid protomer in a simulation of an isolated protomer.

5. Conclusions

The energy parameters of WIN52084s in all-atom approximations have been determined with 6-31G* calculations and the two-conformational two-stage fit method. Using the parameters, the MD simulation of a rhinovirus capsid bound with WIN52084s was performed under rotational symmetry boundary conditions. The simulational trajectory was analyzed mainly from the structural view points. The rms deviations of WIN52084s, the pocket, and the protomer were decomposed to conformational, translational, and rotational components. The translation was further decomposed to radial, longitudinal, and lateral components. The conformational changes of the pocket and WIN52084s were found to be small, indicating good equilibration of their conformation in this large MD simulation, although the pocket cavity was becoming narrower from energetic analysis of the non-bonded energy of WIN52084s. Because motion of the position of WIN52084s in the pocket was similar to that of white noise, the translation of WIN52084s was also well equilibrated. The pocket translation was primarily in the radial and lateral directions, which were perpendicular to the direction of binding for WIN52084s. The easiest path of motion for WIN52084s was on the longitudinal line, providing a track for the binding process of the anti-rhinovirus drug so that it can enter the pocket over a long period. In addition, the continuous shrinking of 0.61 Å was observed for the capsid. The radius of the capsid oscillated with an amplitude of 0.18 Å and a period of 18 ps. The shrinking may be a result of omitting the inner RNA structure. The radial oscillation can be explained as a standing wave based on the elastic shell model.

Acknowledgements

We are highly appreciative of the Institute of Molecular Science, Okazaki, Japan, for the used of their computer facility.

Appendix A

The 18 ps oscillation of a rhinovirus capsid can be explained with the following simple elastic shell model. As written in textbooks on elasticity [33], the radial component of the displacement vector, u_r, in spherically symmetric, isotropic, and elastic media can be expressed as $u_r = \varphi'$, where $\varphi(r, t)$ is a displacement potential, r is the distance from the center of spherical symmetry, and t is the time. φ' denotes the derivative of φ by r. The equation of motion expressed in terms of φ is the following wave function:

$$c^2 \Delta\varphi = \ddot{\varphi} \tag{A.1}$$

where c is the velocity of a plane longitudinal elastic wave, and $\ddot{\varphi}$ is the second derivative of φ by time. Because φ depends on only t and r, $\Delta\varphi$ is equal to $(r^2\varphi')'/r^2$. For oscillations periodic in time ($\varphi(r, t) \propto \exp(-i\omega t)$) with an angular frequency ω, the solution of Eq. (A.1) is given by

$$\varphi = \frac{A \sin(kr + B) \exp(-i\omega t)}{r} \tag{A.2}$$

where k is defined as ω/c. A and B are constants to be determined. Eq. (A.2) is substituted into the following formula of the radial diagonal component, σ_{rr}, of the stress tensor:

$$\sigma_{rr} = \rho\{(c^2 - 2c_t^2)\,\Delta\varphi + 2c^2\varphi''\} \tag{A.3}$$

where φ'' is the second derivative of φ by r, and c_t is the velocity of the plane transverse wave. After the substitution, σ_{rr} is expressed as

$$\sigma_{rr} = -A\rho \left\{ \frac{(\omega^2 - 4c_t^2)\sin(kr + B)}{r + 4c_t^2 k \cos(kr + B)} \right\} \exp(-i\omega t) \tag{A.4}$$

Because σ_{rr} must be null on the surface of elastic media, the following two boundary conditions must be satisfied for a spherical shell with an inner radius of R_1 and an outer radius of R_2:

$$\tan\left(\frac{kR_1 + B}{kR_1}\right) = \left\{1 - \left(\frac{kR_1 c}{2c_t}\right)^2\right\}^{-1} \tag{A.5}$$

$$\tan\left(\frac{kR_2 + B}{kR_2}\right) = \left\{1 - \left(\frac{kR_2 c}{2c_t}\right)^2\right\}^{-1} \tag{A.6}$$

The above concurrent equations on B and k can be solved by a minor numerical calculation. As a result, ω that is equal

to ck is dependent only on R_1, R_2, c, and ratio, c:c_t. For a rhinovirus capsid, R_1 is about 110 Å and R_2 is about 160 Å, c ranges from 2000 to 6500 m/s, and c:c_t ranges from 1.8 to 2.5 for most kinds of solid, including iron, zinc, glass, nylon, and polystyrene [34]. Using these values, the smallest solution of ω in Eqs. (A.5) and (A.6) ranges from 0.19 to 0.72 rad/ps. Therefore, the period of the slowest standing wave of the shell is in a range of 8.8–34 ps, and the 18 ps period of the radial oscillation in our simulation is just within the range. In the above calculation, the elasticity of water that surrounds the capsid was neglected because the self-diffusion coefficient of water [35,36] ranges from 2×10^{-5} to 4×10^{-5} cm^2/s, and a water molecule randomly travels over an area of 10–15 Å in 10 ps, so water can be considered to be fluid in this problem about 18 ps oscillation.

References

[1] B.N. Fields, D.M. Knipe, P.M. Howley (Eds.), Fields Virology, Lippincott-Raven, Philadelphia, 1996.

[2] W. Chiu, R.M. Burnett, R.L. Garcea (Eds.), Structural Biology of Viruses, Oxford University Press, New York, 1997.

[3] G.D. Diana, D.C. Pevear, Antipicornavirus drugs: current status, Antiviral Chem. Chemotherapy 8 (1997) 401–408.

[4] D.K. Phelps, C.B. Post, A novel basis for capsid stabilization by antiviral compounds, J. Mol. Biol. 254 (1995) 544–551.

[5] D.K. Phelps, P.J. Rossky, C.B. Post, Influence of an antiviral compound on the temperature dependence of viral protein flexibility and packing: a molecular dynamics study, J. Mol. Biol. 274 (1998) 331–337.

[6] D.K. Phelps, C.B. Post, Molecular dynamics investigation of the effect of an antiviral compound on human rhinovirus, Protein Sci. 8 (1999) 2281–2289.

[7] D.K. Phelps, B. Speelman, C.B. Post, Theoretical studies of viral capsid proteins, Curr. Opin. Struct. Biol. 10 (2000) 170–173.

[8] B. Speelman, B.R. Brooks, C.B. Post, Molecular dynamics simulations of human rhinovirus and an antiviral compound, Biophys. J. 80 (2001) 121–129.

[9] A.W. Dove, V.R. Racaniello, An antiviral compound that blocks structural transitions of poliovirus prevents receptor binding at low temperatures, J. Virol. 74 (2000) 3929–3931.

[10] T. Cagin, M. Holder, B.M. Pettitt, A method for modeling icosahedral virions: rotational symmetry boundary conditions, J. Comput. Chem. 12 (1991) 627–634.

[11] S. Yoneda, M. Kitazawa, H. Umeyama, Molecular dynamics simulation of a rhinovirus capsid under rotational symmetry boundary conditions, J. Comput. Chem. 17 (1996) 191–203.

[12] S. Yoneda, A further implementation of the rotational symmetry boundary conditions for calculations of $P4_32_12$ symmetry crystals, J. Mol. Graphics Modell. 15 (1997) 233–237.

[13] T. Yoneda, S. Yoneda, N. Takayama, M. Kitazawa, H. Umeyama, A homology modeling method of an icosahedral viral capsid: inclusion of surrounding protein structures, J. Mol. Graphics Modell. 17 (1999) 114–119.

[14] M. Levitt, Molecular dynamics of native protein. Part I. Computer simulation of trajectoriesm, J. Mol. Biol. 168 (1983) 595–620.

[15] M. Levitt, Molecular dynamics of native protein. Part II. Analysis and nature of motion, J. Mol. Biol. 168 (1983) 621–657.

[16] A. Warshel, Bicycle-pedal model for the first step in the vision process, Nature 260 (1976) 679–683.

[17] W.F. Lau, B.M. Pettitt, T.P. Lybrand, Molecular dynamics of coat proteins of the human rhinovirus, Mol. Simul. 1 (1988) 385–398.

[18] T.P. Lybrand, J.A. McCammon, Computer simulation study of the binding of an antiviral agent to a sensitive and a resistant human rhinovirus, J. Comput. Aided Mol. Des. 2 (1988) 259–266.

[19] W.F. Lau, B.M. Pettitt, Dynamics of an oxazole compound bound to a common cold virus, J. Am. Chem. Soc. 111 (1989) 4111–4113.

[20] R.C. Wade, J.A. McCammon, Binding of an antiviral agent to a sensitive and a resistant human rhinovirus computer simulation studies with sampling of amino acid side-chain conformations. Part I. Mapping the rotamers of residue 188 of viral protein 1, J. Mol. Biol. 225 (1992) 679–696.

[21] R.C. Wade, J.A. McCammon, Binding of an antiviral agent to a sensitive and a resistant human rhinovirus computer simulation studies with sampling of amino acid side-chain conformations. Part II. Calculation of free energy differences by thermodynamic integration, J. Mol. Biol. 225 (1992) 697–712.

[22] W.D. Cornell, P. Cieplak, C.L. Bayly, I.R. Gould, K.M. Merz Jr., D.M. Ferguson, D.C. Spellmeyer, T. Fox, J.W. Caldwell, P.A. Kollman, A second generation force field for the simulation of proteins nucleic acids and organic molecules, J. Am. Chem. Soc. 117 (1995) 5179–5197.

[23] P. Kollman, R. Dixon, W. Cornell, T. Fox, C. Chipot, A. Pohorille, The development/application of a minimalist organic/biochemical molecular mechanic force field using a combination of ab initio calculations and experimental data, in: W.F. van Gunsteren, P.K. Weiner, A.J. Wilkinson (Eds.), Computer Simulation of Biomolecular Systems: Theoretical and Experimental Applications, Vol. 3, Kluwer Academic Publishers, London, 1997, pp. 83–96.

[24] J. Badger, L. Minor, M.J. Kremer, M.A. Oliveira, T.J. Smith, J.P. Griffith, D.M.A. Guerin, S. Krishnaswamy, M. Luo, M.G. Rossmann, M.A. Mckinlay, G.D. Diana, F.J. Dutko, M. Fancher, R.R. Rueckert, B.A. Heinz, Structural analysis of a series of antiviral agents complexed with human rhinovirus 14, Proc. Natl. Acad. Sci. U.S.A. 85 (1988) 3304–3308.

[25] H.M. Berman, J. Westbrook, Z. Feng, G. Gilliland, T.N. Bhat, H. Weissig, I.N. Shindyalov, P.E. Bourne, The protein data bank, Nucl. Acids Res. 28 (2000) 235–242.

[26] Gaussian'98, Gaussian, Inc., Carnegie, Pittsburgh, 1998.

[27] C.I. Bayly, P. Cieplak, W.D. Cornell, P.A. Kollman, A well-behaved electrostatic potential based method using charge restraints for deriving atomic charges: the RESP model, J. Phys. Chem. 97 (1993) 10269–10280.

[28] W.D. Cornell, P. Cieplak, C.I. Bayly, P.A. Kollman, Application of RESP charges to calculate conformational energies, hydrogen bond energies, and free energies of solvation, J. Am. Chem. Soc. 115 (1993) 9620–9631.

[29] D.A. Case, D.A. Pearlman, J.W. Caldwell, T.E. Cheatham, III, W.S. Ross, C.L. Simmerling, T.A. Darden, K.M. Merz, R.V. Stanton, A.L. Cheng, J.J. Vincent, M. Crowley, V. Tsui, R.J. Radmer, Y. Duan, J. Pitera, I. Massova, G.L. Seibel, U.C. Singh, P.K. Weiner, P.A. Kollman, AMBER6, University of California, San Francisco, 1999.

[30] S. Yoneda, H. Umeyama, Free energy perturbation calculations on multiple mutation bases, J. Chem. Phys. 97 (1992) 6730–6736.

[31] J.-P. Ryckaert, G. Cicotti, H.J.C. Berendsen, Numerical integration of the Cartesian equation of motion of a system with constraints: molecular dynamics of n-alkanes, J. Comput. Phys. 23 (1977) 327–341.

[32] H.J.C. Berendsen, J.P.M. Postma, W.F. van Gunsteren, A. DiNola, J.R. Haak, Molecular dynamics with coupling to an external bath, J. Chem. Phys. 81 (1984) 3684–3690.

[33] L.D. Landau, E.M. Lifshitz, Theory of Elasticity, Course of Theoretical Physics, Vol. 7, 3rd Edition, Pergamon, New York, 1986 (Chapter 3).

[34] D.R. Lide (Ed.), Handbook of Chemistry and Physics, 75th Edition, CRC Press, Florida, 1994.

[35] D. Eisenberg, W. Kauzmann, The Structure and Properties of Water, Oxford University Press, London, 1969.

[36] A. Rahman, F.H. Stillinger, Molecular dynamics study of liquid water, J. Chem. Phys. 55 (1971) 3336–3359.